CHEMISTRY OF MATERIALS
Article

Chem. Mater. **2010,** *22,* 4103–4110 4103
DOI:10.1021/cm1010967

Magnetic Hardness of $Fe_{60}Pt_{40}$ Nanoparticles Controlled by Surface Chemistry

David Serantes,[†] Marina Spasova,[‡] Daniel Baldomir,[†] Michael Farle,[‡] and Veronica Salgueirino*[,§]

[†]*Departamento de Física Aplicada e Instituto de Investigacións Tecnolóxicas, Universidade de Santiago de Compostela, 15782, Santiago de Compostela, Spain,* [‡]*Fakultät für Physik and Center for Nanointegration (CeNIDE), Universität Duisburg-Essen, Germany, and* [§]*Departamento de Física Aplicada, Universidade de Vigo, 36310 Vigo, Spain*

Received April 20, 2010. Revised Manuscript Received May 21, 2010

$Fe_{60}Pt_{40}$ nanoparticles stabilized by oleic acid/oleylamine or tetramethylammonium hydroxide and self-assembled in 3D dispersions permit a detailed analysis of the competition of surface, finite-size effects and magnetic interparticle interactions which controls the collective macroscopic magnetic behavior. Temperature dependent magnetometry demonstrates that for FePt nanoparticles with identical size distribution but different surface chemistry, substantial differences of the effective magnetic anisotropy exist and can be understood by comparison with different theoretical models. Finally, a model yielding quantitative data for the competing intrinsic magnetic parameters of complex core−shell nanoparticles is derived.

Introduction

The structural and magnetic properties of monodisperse Fe_xPt_{1-x} nanoparticles have been the subject of intense research activity over the past few years because of their potential for usage in biomedical theranostic and magnetic data storage as well as magnetic sensor applications.[1−6] The established methods of wet-chemistry synthesis of FePt nanoparticles yield highly controllable particle sizes, compositions, and morphologies as well as narrow size distributions. These FePt particles are in the chemically disordered fcc structure, which is characterized by a very small magnetic anisotropy energy density (MAE) and soft magnetic properties.[7−11] Small modifications of the crystalline structure and composition are known to result in large changes in the MAE and the intrinsic magnetic correlations, rendering these nanoparticulate systems attractive prototype models for understanding nanomagnetism.[12,13]

Theoretical descriptions of the macroscopic magnetic response of nanoparticulate assemblies rely intrinsically upon the accurate knowledge of the effective magnetic anisotropy density K_{eff}, the volume, and the magnetic dipolar interaction strengths of the particles. Acquisition of such values is, however, notoriously difficult.[14] Additionally, surface effects (generally controlled by the molecular ligands attached) dominate their magnetic properties because of the increased surface-to-volume ratio of fine nanoparticles.[15,16] The surface magnetism differs from volume properties due to the lower coordination of magnetic moments and the breaking of symmetry at the surface.[17,18] This can result in site-specific, generally uniaxial, surface anisotropy and broken exchange bonds, which inevitably lead to surface spin disorder and frustration (most prominently in oxidic ferro-, antiferro-, and ferrimagnets).[19] In terms of surface chemistry, FePt nanoparticles offer an excellent chemical stability that allows surfactant exchange and/or (bio)molecules attachment,

*Corresponding author. E-mail: vsalgue@uvigo.es.

(1) Weller, D.; Moser, L.; Folks, L.; Best, M. E.; Lee, W.; Toney, M. F.; Schwickert, M.; Thiele, J.-U.; Doerner, M. F. *IEEE Trans. Magn.* **2000**, *36*, 10.
(2) Zeng, H.; Sun, S.; Vedantam, T. S.; Liu, J. P.; Dai, Z.-R.; Wang, Z.-L. *Appl. Phys. Lett.* **2002**, *80*, 2583.
(3) Lee, D. C.; Mikulec, F. V.; Pelaez, J. M.; Koo, B.; Korgel, B. A. *J. Phys. Chem. B* **2006**, *110*, 11160.
(4) Sort, J.; Suriñach, S.; Baró, M. D.; Muraviev, D.; Dzhardimalieva, G. I.; Golubeva, N. D.; Pomogailo, S. I.; Pomogailo, A. D.; Macedo, W. A. A.; Weller, D.; Skumryev, V.; Nogués, J. *Adv. Mater.* **2006**, *18*, 466.
(5) Y. Zhang, Y.; Wan, J.; Skumrev, V.; Stoyanov, S.; Huang, Y.; Hadjipanayis, G. C.; Weller, D. *Appl. Phys. Lett.* **2004**, *85*, 5343.
(6) Sun, S. *Adv. Mater.* **2006**, *18*, 393.
(7) Sun, S.; Murray, C. B.; Weller, D.; Folks, L.; Moser, A. *Science* **2000**, *287*, 1989.
(8) Chen, M.; Liu, J. P.; Sun, S. *J. Am. Chem. Soc.* **2004**, *126*, 8394.
(9) Howard, L. E. M.; Nguyen, H. L.; Giblin, S. R.; Tanner, B. K.; Terry, I.; Hughes, A. K.; Evans, J. S. O. *J. Am. Chem. Soc.* **2005**, *127*, 10140.
(10) Elkins, K. E.; Vendantam, T. S.; Liu, J. P.; Zeng, H.; Sun, S.; Wang, Z. L.; Ding, Y. *Nano Lett.* **2003**, *3*, 1647.
(11) Wiedwald, U.; Spasova, M.; Salabas, E. L.; Ulmeanu, M.; Farle, M.; Frait, Z.; Fraile-Rodriguez, A.; Arvanitis, D.; Sobal, N. S.; Higendorff, M.; Giersig, M. *Phys. Rev. B* **2003**, *68*, 644241.
(12) Antoniak, C.; Lindner, J.; Spasova, M.; Sudfeld, D.; Acet, M.; Farle, M.; Fauth, K.; Wiedwald, U.; Boyen, H.-G.; Ziemann, P.; Wilhelm, F.; Rogalev, A.; Shouheng, S. *Phys. Rev. Lett.* **2006**, *97*, 117201.
(13) Antoniak, C.; Farle, M. *Mod. Phys. Lett. B* **2007**, *21*, 1111.
(14) Wiedwald, U.; Lindner, J.; Spasova, M.; Frait, Z.; Farle, M. *Phase Transitions* **2005**, *78*, 85.
(15) Vestal, C. R.; Zhang, Z. J. *J. Am. Chem. Soc.* **2003**, *125*, 9828.
(16) Shukla, N.; Liu, C.; Jones, P. M.; Weller, D. *J. Magn. Magn. Mater.* **2003**, *266*, 178.
(17) Néel, L. *J. Phys. Radium* **1954**, *15*, 225.
(18) Farle, M.; Platow, W.; Anisimov, A. N.; Schulz, B.; Baberschke, K. *J. Magn. Magn. Mater.* **1997**, *165*, 74.
(19) Iglesias, O.; Labarta, A. *Phys. Rev. B* **2001**, *63*, 184416.

Published on Web 06/08/2010

permitting for example their transfer from nonpolar solvents to aqueous solution.[20] This method opens the door not only to biological applications[21] but also to the water-based colloidal chemistry of FePt nanostructures.[22]

Moreover, the collective magnetic behavior of a nanoparticle assembly is generally investigated using a nonmagnetic matrix or solvent.[23−29] Magnetic interactions between particles can be due to dipolar, direct, or indirect exchange coupling.[30] In some circumstances, interactions can dominate the magnetic behavior, resulting in an ordered or disordered magnetic state of the nanoparticle ensemble, for example, "spin-glass-like" ordering of magnetic moments.[31]

In this work, we investigated two types of ligand-stabilized $Fe_{60}Pt_{40}$ nanoparticles that promote different three-dimensional (3D) self-assemblies and distances in between. A detailed analysis and comparison of the magnetic properties of these FePt nanoparticles with identical size distribution but different surface chemistry is reported, proving experimentally the substantial differences in the effective magnetic anisotropy. Our extensive analysis of the magnetic behavior of the nanoparticulate systems excludes a leading role of interparticle interactions or the different random or face-centered cubic (fcc) spatial distribution; instead, the rather different individual particle characteristics promoted by the surface conditions dominate.

Experimental Section

$Fe_{60}Pt_{40}$ nanocrystals were synthesized following the method published by Sun and co-workers.[7] Under airless conditions, platinum acetylacetonate (0.5 mmol) and 1,2-hexadecandiol (1.5 mmol) were dissolved in 20 mL of dioctyl ether and heated to 100 °C. Oleic acid (0.5 mmol), oleylamine (0.5 mmol), and iron pentacarbonyl (0.5 mmol) were added to the mixture, which was subsequently heated further up to 288 °C. The solution was maintained at reflux for 1 h and then cooled to room temperature. All handling thereafter was performed open to the atmosphere. Upon completion of the synthesis, the nanoparticles were subjected to successive washing cycles to remove excess surfactant from solution. In each cycle, 40 mL of ethanol were added to the mixture, causing the nanoparticles to precipitate under centrifugation. The supernatant was discarded, and the nanoparticles were redispersed in hexane (20 mL) in the presence of oleic acid (0.05 mL) and oleylamine (0.05 mL). This sequence was repeated three times.

The precipitation of the synthesized nanoparticles (5 mL of hexane-based solution, 0.01 g/mL) was accomplished by the addition of ethanol followed by centrifugation. The supernatant was then discarded, and the precipitate was redispersed in a mixture of 2 mL of tetramethylammonium hydroxide (TMAOH) (10 wt % in H_2O)[20] and 100 mL of deionized water. By brief shaking followed by sonication for 5 min, the nanoparticles were completely redispersed in water, and only a small amount of aggregated clusters settled down after some hours, leaving a dark (but not turbid) solution of FePt nanoparticles in the water. The FePt nanoparticles in water were centrifuged several times in order to eliminate the excess of surfactants, and the precipitate was again redispersed in 40 mL of TMAOH solution (0.01 wt %).

The same $Fe_{60}Pt_{40}$ nanoparticles stabilized in hexane using oleic acid and oleylamine were subsequently transferred and modified with hydroxide ions thereby reducing errors resulting from possible batch-dependent variations of shape, size, and composition. In the hexane-based solution, FePt nanoparticles are stabilized with alkyl carboxylic acid and amine, which link covalently to Fe or by a coordination bond to Pt, respectively.[32] In the water-based solution, FePt nanoparticles are stabilized with TMAOH, which provides each particle with an electrostatic double layer, rendering the nanoparticles fully dispersible in aqueous solution.[20]

TEM measurements were performed on a Philips CM12 instrument operating at an acceleration voltage of 120 kV. Samples for TEM were prepared by placing a drop of FePt nanoparticle dispersions on a Cu grid and letting the liquid evaporate at room temperature. To study the magnetic properties using a superconducting quantum interference device (SQUID) magnetometry the FePt nanoparticles were precipitated from the corresponding water- and hexane-based solutions. The dried, loosely packed powder samples in which the interparticle distance is given by the ligands at their surface were measured lodged into straws in a Quantum Design SQUID Magnetometer. The samples will be denoted as (H) in the case of hexane-based, and (W) in the case of water-based FePt nanoparticles.

Results and Discussion

Figure 1a shows the log-normal size distribution of the FePt nanoparticles yielding a standard deviation of 13% and a mean size of 3.6 nm. We find that based on the type of ligands at their surface, the particles self-assemble at room temperature in a hexagonal close-packed array in the case of sample H and randomly organized in the case of sample W (Figure 1b,c). The TEM images show nonagglomerated self-assembled or randomly distributed particles even after the phase transfer. For FePt nanoparticles dispersed in hexane, the alkyl chain of the ligands (oleic acid/oleylamine) is very mobile because of the high curvature of the nanoparticles surface. This ensures the stability of the colloidal solution. If the particles get closer to each other when the solvent evaporates, the motion of the alkyl chain becomes more and more restricted, energetically favoring an interdigitation process due to van der Waals interactions of the alkyl chains and inducing partial crystallization of the particles. Indeed, nanoparticles with narrow size distributions can form

(20) Salgueiriño-Maceira, V.; Liz-Marzán, L. M.; Farle, M. *Langmuir* **2004**, *20*, 6946.
(21) Gu, H.; Ho, P.-L.; Tsang, K.W. T.; Wang, L.; Xu, B. *J. Am. Chem. Soc.* **2003**, *125*, 15702.
(22) Salgueiriño-Maceira, V.; Correa-Duarte, M. A.; Farle, M. *Small* **2005**, *1*, 1073.
(23) Wiedwald, U.; Cerchez, M.; Farle, M.; Fauth, K.; Schütz, G.; Zürn, K.; Boyen, H.-G.; Ziemann, P. *Phys. Rev B* **2004**, *70*, 214412.
(24) Djurberg, C.; Svedlindh, P.; Nordblad, P.; Hansen, M. F.; Bodker, F.; Morup, S. *Phys. Rev. Lett.* **1997**, *79*, 5154.
(25) Luo, W.; Nagel, S. R.; Fosenbaum, T. F.; Rosensweig, R. E. *Phys. Rev. Lett.* **1991**, *67*, 2721.
(26) Jonsson, T.; Mattsson, J.; Djurberg, C.; Khan, F. A.; Nordblad, P.; Svedlindh, P. *Phys. Rev. Lett.* **1995**, *75*, 4138.
(27) Salgueiriño-Maceira, V.; Correa-Duarte, M. A.; Duman, E.; Farle, M. *J. Magn. Magn. Mater.* **2006**, *299*, 467.
(28) Hoppe, C. E.; Rivadulla, F.; Vidal-Vidal, J.; López-Quintela, M. A.; Rivas, J. *J. Nanosci. Nanotechnol.* **2008**, *8*, 2883.
(29) Hoppe, C. E.; Rivadulla, F.; López-Quintela, M. A.; Bujan, M. C.; Rivas, J.; Serantes, D.; Baldomir, D. *J. Phys. Chem. C* **2008**, *112*, 13099.
(30) Baldomir, D.; Serantes, D.; Pereiro, M.; Botana, J.; Arias, J. E.; Masunaga, S. H.; Rivas, J. *J. Nanosci. Nanotechnol.* **2010**, *10*, 2717.
(31) Salgueiriño-Maceira, V.; Correa-Duarte, M. A.; Bañobre-López, M.; Grzelczak, M.; Farle, M.; Liz-Marzán, L. M.; Rivas, J. *Adv. Funct. Mater.* **2008**, *18*, 616.
(32) Shukla, N.; Ahner, J.; Weller, D. *J. Magn. Magn. Mater.* **2004**, *272−276*, e1349.

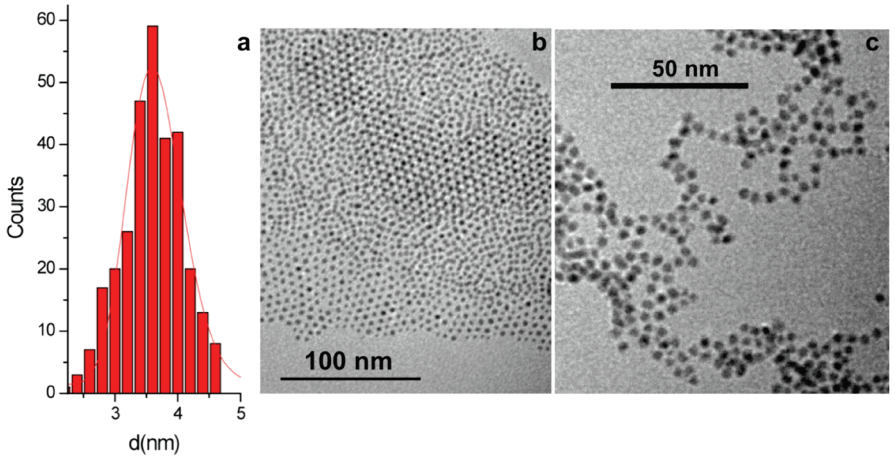

Figure 1. (a) Size distribution analysis and TEM micrographs of the FePt nanoparticles from samples (b) H and (c) W.

close-packed arrays on a variety of substrates.[33,34] The FePt nanoparticles stabilized with oleic acid and oleylamine behave as building blocks for superlattices, driven by van der Waals and possibly also by magnetic interactions,[35] as shown in Figure 1b. The interparticle spacing given by the C_{18} chains of the ligands is ~2.5 nm in the dry state. With shorter surfactants such as hexanoate/hexylamine the interparticle distance decreases to ~1 nm.[32] In sample W, using the TMAOH as surfactant, the crystallization process is highly inhibited. TMAOH lacks the characteristic hydrocarbon chain, so that the interparticle distance is much smaller than 1 nm, additionally favoring strong electrostatic interactions between the ions at the surface of the nanoparticles and therefore preventing the crystalline ordering.

The densest possible volume packing fraction ϕ for identical spheres is $\phi = \pi/\sqrt{18} \approx 0.74$, corresponding to the close-packed fcc lattice. In sample H, the ligands keep the nanoparticles even in close-packed fcc structure about 2.5 nm apart, and the packing fraction can only reach $\phi = 0.15$. In the case of sample W, the FePt nanoparticles reorganize into a disordered structure as the solvent evaporates so that the processes leading to random packing become important.[36] Considering colloidal nanoparticles, which are less affected by the gravitational acceleration, and taking into account interparticle forces like ideally repulsive hard-sphere interactions, magnetic interactions, entropic forces, and/or friction between the particles, which inhibits densification, the precise proportion of each of these competing effects is difficult to quantify, as demonstrated by Torquato et al., who proposed a maximally random jammed state with the maximum packing density $\phi \approx 0.64$.[37] However, taking into account that the TMAOH molecules keep the nanoparticles < 1 nm apart, we find $\phi \approx 0.31$.

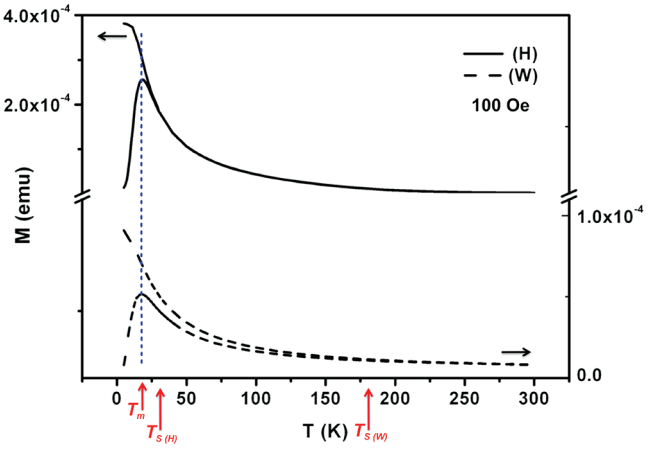

Figure 2. ZFC-FC magnetization curves of the FePt nanoparticles from sample H (solid line) and sample W (dashed line).

Figure 2 shows zero-field-cooled (ZFC) magnetization curves recorded after cooling the samples in zero field from room temperature to 5 K and field-cooled (FC) curves recorded after cooling the samples in a small field (100 Oe). These ZFC-FC magnetization curves display the usual signatures observed in single-domain magnetic particle systems. For both samples, the curves coincide at high temperatures and exhibit a paramagnetic-like decay with increasing temperature, reflecting the superparamagnetic response of the particles within the time window of the measurement technique.[38] With decreasing temperature, the curves split; the ZFC reaches a maximum at $T_m = 18$ K that roughly corresponds to the average blocking temperature T_B of the system and decreases after that, whereas the FC one keeps increasing. The slope of the curves is less-pronounced for the more densely packed sample W consistent with the existence of larger dipolar coupling[30,39] and larger size and anisotropy dispersions. The maximum of the ZFC curve is proportional to the individual particles' anisotropy energy barriers E_B (proportional to the particle magnetic anisotropy K and volume V of the particles) in a first approximation.

(33) Dumestre, F.; Martínez, S.; Zitoun, D.; Fromen, M.-C.; Casanove, M.-J.; Lecante, P.; Respaud, M.; Serres, A.; Benfield, R. E.; Amiens, C.; Chaudret, B. *Faraday Discuss.* **2004**, *125*, 265.
(34) Talapin, D. V.; Shevchenko, E. V.; Kornowski, A.; Gaponik, N.; Haase, M.; Rogach, A. L.; Weller, H. *Adv. Mater.* **2001**, *13*, 1868.
(35) Spasova, M.; Wiedwald, U.; Ramchal, R.; Farle, M.; Hilgendorff, M.; Giersig, M. *J. Magn. Magn. Mater.* **2002**, *240*, 40.
(36) Jaeger, H. M.; Nagel, S. R. *Science* **1992**, *255*, 1524.
(37) Torquato, S.; Truskett, T. M.; Debenedetti, P. G. *Phys. Rev. Lett.* **2000**, *84*, 2064.
(38) Antoniak, C.; Lindner, J.; Farle, M. *Europhys. Lett.* **2005**, *70*, 250.
(39) Respaud, M.; Broto, J. M.; Rakoto, H.; Ousset, J. C.; Osuna, J.; Oud Ely, T.; Amiens, C.; Chaudret, B.; Askenazy, S. *Physica B* **1998**, *246*−*247*, 532.

For typical SQUID measurements T_B is given by the equation $T_B \approx E_B/25k_B$, where k_B is the Boltzmann constant (see eq 3). Therefore, dispersion in the magnetic anisotropy K and volume V among the particle population results in dispersion of the corresponding E_B, and thereby in a less-pronounced peak of the ZFC curve. The effect of this distribution in the particles' energy barriers can also be induced by interparticle dipole−dipole interactions.

As pointed above, T_m depends only on the average particle size if the magnetic anisotropy energy density K is size independent. The temperature ($T_{S(H)} = 23$ K in the case of sample H and $T_{S(W)} \approx 182$ K in sample W) at which the ZFC and FC curves separate corresponds to the T_B of the largest particles. This could imply that the average volume or K of the nanoparticles in sample W has increased when transferred to the aqueous solution, but an increase in volume was not evident from the TEM analysis after the phase transfer.

It is very important to remember that a distribution of blocking temperatures stems not only from a size distribution as has been suggested in several publications but more precisely from a distribution of energy barriers E_B, i.e., a distribution of particle sizes and/or magnetic anisotropy energy densities. The shape of the ZFC curve, with its initial increase until T_B is reached, is also observed in fully monodisperse samples. In fact, because the relaxation time τ for a single particle is given by eq 1, every particle has a nonvanishing temperature-dependent probability $f(T)$ (eq 2) for a reversal of its magnetization at any temperature.

$$\tau = \tau_0 e^{E_B/k_B T} \tag{1}$$

$$f(T) = \tau^{-1}(T) = f_0 e^{-E_B/k_B T} \tag{2}$$

One has to distinguish the temperature T_0 of the energy barrier $E_B = k_B T_0$ from the temperature at which their magnetization reverses according to the thermal probability expressed by eq 2. Obtaining a precise picture of the distribution of switching rates is quite complicated because of the random spatial distribution of easy axes.

Most of the single-particle properties are indeed hidden by the complex distribution function of the MAE, resulting from different particle sizes, shapes and even compositions. In sample W, this distribution stems from the partial and heterogeneous oxidation of the nanoparticles when transferred to the aqueous solution. The effect of oxidation induced changes that have been analyzed for example by Wiedwald et al.[40] for cobalt nanoparticles. Nogues et al. also discussed the drawback of having antiferromagnetic (AFM) shells that usually grow highly disordered, making the control of its microstructure rather difficult.[41] How these surface oxides of transition metal nanoparticles affect the magnetic properties has been a subject of intensive research. The oxides are usually AFM and can introduce extra sources of anisotropy due to uncompensated magnetic moments, grain size distribution, structural defects, interfacial roughness, and variations in the chemical composition.[40−42] As can be directly understood in terms of Néel's pair model, the surface anisotropy is mainly due to local symmetry breaking at the surface and structural defects.[43] In the two systems under study (samples H and W), these contributions clearly differ.

The increase of T_S in sample W can be explained by a combination of increased interparticle interactions and a broader distribution of effective magnetic anisotropy constants (K_{eff}) compared to sample H. Both contributions are a direct consequence of the different chemical compounds surrounding the nanoparticles. Samples H and W have a differently dense volume fraction, of ∼15 and ∼31% assuming a face centered cubic superstructure and a maximally random jammed state, respectively. The ligands also dictate the chemistry at the surface of the nanoparticles. A partial oxidation of Fe atoms is expected due to handling sample H under air atmosphere but a thicker irregular oxide shell in sample W forming a core−shell FePt-(Fe_xO_y)Pt nanoparticle is likely, because of the hydroxide ions at the surface and the oxygen-rich environment using water as solvent. Under these conditions, particle surface and core effects are not easily distinguished and contribute to the magnetic behavior of nanoparticles in a nonseparatable way.[41] The difference in the T_S of the two samples ($T_{S(H)} = 23$ K, $T_{S(W)} = 182$ K) is consequently not because of an increase in size but related to an increase of the effective MAE distribution. The very thin, possibly incomplete AFM shell around the FM core varies from particle to particle[40] and results in a broader distribution of MAE, relaxation times and blocking processes. The latter are strongly influenced by dipolar coupling effects as the temperature is lowered.

The experimentally determined mean particle volume V_m and T_B can be used to roughly estimate K_{eff} considering that for typical SQUID measurements $\ln(\tau_m/\tau_0) \approx 25$, by

$$K_{eff} = \frac{25k_B T_B}{V_m} \tag{3}$$

where k_B is the Boltzmann's constant. Unfortunately, an unambiguous determination by measuring the magnetization in a different time window of relaxation processes[38] was not possible.[44] For very fine particles, it is unlikely that their "magnetic" or "activation" mean volume V_m is the same as their geometric volume. In the case of sample W, as the surface layers may be quite thin and even incomplete the

(40) Wiedwald, U.; Fauth, K.; Hebler, M.; Boyen, H.-G.; Weigl, F.; Hilgendorff, M.; Giersig, M.; Schütz, G.; Ziemann, P.; Farle, M. *ChemPhysChem* **2005**, *6*, 2522.
(41) Nogues, J.; Sort, J.; Langlais, V.; Skumryev, V.; Suriñach, S.; Muñoz, J. S.; Baró, M. D. *Phys. Rep* **2005**, *422*, 65.
(42) Ozatay, O.; Gowtham, P. G.; Tan, K. W.; Read, J. C.; Mkhoyan, K. A.; Thomas, M. G.; Fuchs, G. D.; Braganca, P. M.; Ryan, E. M.; Thadani, K. V.; Silcox, J.; Ralph, D. C.; Buhrman, R. A. *Nat. Mater.* **2008**, *7*, 567.
(43) Salazar-Alvarez, G.; Qin, J.; Sepelak, V.; Bergmann, I.; Vasilakaki, M.; Trohidou, K. N.; Ardisson, J. D.; Macedo, W. A. A.; Mikhaylova, M.; Muhammed, M.; Baró, M. D.; Nogues, J. *J. Am. Chem. Soc.* **2008**, *130*, 13234.
(44) Holmes, B. M.; Newman, D. M.; Wears, M. L. *J. Magn. Magn. Mater.* **2007**, *315*, 39.

irregular increase of the surface anisotropy and a decrease in the magnetocrystalline anisotropy energy due to the reduced core size become important. This model fits indeed, if most of the particles are modeled by an oxidized surface layer unable to form a crystalline AFM phase, and the atomic moments form a magnetically frustrated shell instead. The existence of an AFM phase for a very small fraction of particles only justifies the existence of large energy barriers reflected in the high T_S.

When interpreting the average T_m and the T_S one has to consider the competing influence of the effective magnetic anisotropy density K_{eff}, the saturation magnetization M_S, and the volume V_m of every individual particle, as well as the variation of interparticle interactions (mainly of dipolar type proportional to M_S^2) and average size distribution. As the particles in sample W are much closer packed, we would expect larger interparticle interactions and a shift of T_m to higher temperatures that is not observed. This indicates that the dipolar interaction energy between the particles is rather small in comparison to the MAE, and its contribution to the blocking phenomena is negligible. Also, Monte Carlo simulations (not included) have shown that such different spatial arrangement (fcc or random) would not affect noticeably the shape of the curves in the small dipolar coupling regime. Accordingly, we may conclude that the different behavior arises from the different physical and chemical characteristics of the particles in each sample because of the different ligands at the surface.

For systems of noninteracting nanoparticles, the susceptibility follows a simple Curie law above the blocking temperature, with a deviation from the linear slope at high temperatures due to the temperature dependence of the nanoparticles' magnetic moment.[45] Figure 3 shows the inverse of the susceptibility curves for both samples.

The inverse susceptibility shows different tendencies: (a) for sample H, starting from 20 K, the slope of the $\chi^{-1}(T)$ curve increases up to 220 K and becomes constant, b) for the sample W the slope monotonically decreases before reaching a constant value near room temperature. In order to interpret the magnetic behavior above T_B we consider the characteristic superpara-/paramagnetic (SPM-PM) transition. In a first approximation, the initial susceptibility of a PM system is described by

$$\chi_{PM}(T) = \frac{\rho_{AT}\mu_{AT}^2}{3k_B(T - T_C)} \quad (4)$$

where ρ_{AT} = number of atomic moments μ_{AT} per unit volume. The initial susceptibility χ_{SPM} of a SPM is given by

$$\chi_{SPM}(T) = \frac{\rho_p\mu_p^2}{3k_B(T + T_D)} \quad (5)$$

where μ_p is the total magnetic moment of the particle and ρ_p the number of magnetic particles per unit volume. T_D stands for the effective dipolar interaction energy.[46] Taking into account that each particle is composed to a large extent of different atomic magnetic moments (N) within the PM and the SPM regimes (paramagnetic atomic moments or exchange coupled moments forming coherently fluctuating *supermoments*),

$$\mu_p = N\mu_{AT} \quad (6)$$

,

$$\rho_p = \frac{\rho_{AT}}{N} \quad (7)$$

,in a first approximation, the magnetic susceptibility for the SPM sample is about N times larger than the PM one, because $\chi_{SPM} = N\chi_{PM}$. N is on the order of hundreds or thousands of atoms. Accordingly, the inverse susceptibility must be larger for the system in the PM state than in the SPM one, as reflected in the experimental curves of Figure 3.

The curvature observed in the intermediate temperature (SPM) range accounts for the thermal dependence of the magnetic moment of the nanoparticles, which well-above the blocking temperature satisfactorily follows a mean-field dependence

$$\mu_p(T) = \mu_p(T = 0)\left(1 - \frac{T}{T_C}\right)^{1/2} \quad (8)$$

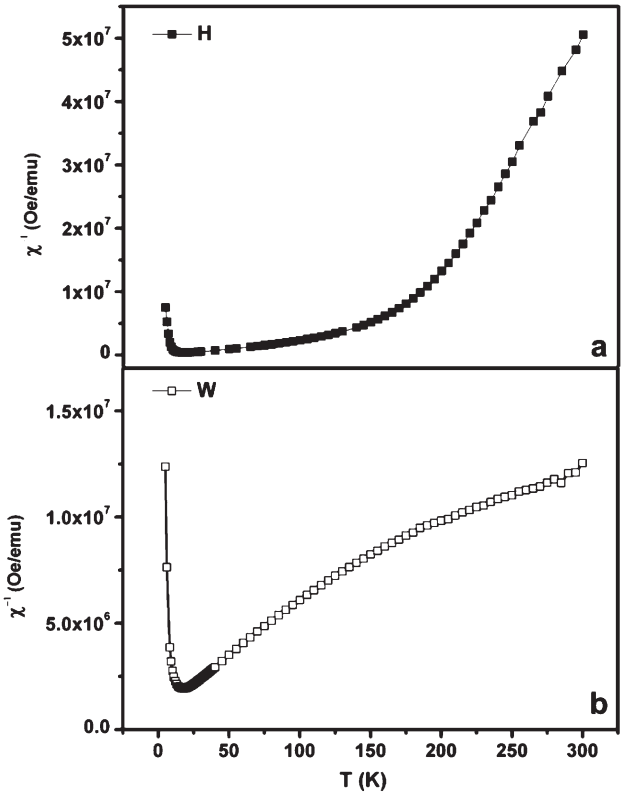

Figure 3. Experimental curves of inverse susceptibility vs temperature for both samples (a) H and (b W) that deviate from the classical Curie law.

(45) Margeat, O.; Tran, M.; Spasova, M.; Farle, M. *Phys. Rev. B* **2007**, *75*, 134410.

(46) Allia, P.; Coisson, M.; Tiberto, P.; Vinai, F.; Knobel, M.; Novak, M. A.; Nunes, W. C. *Phys. Rev. B* **2002**, *64*, 144420.

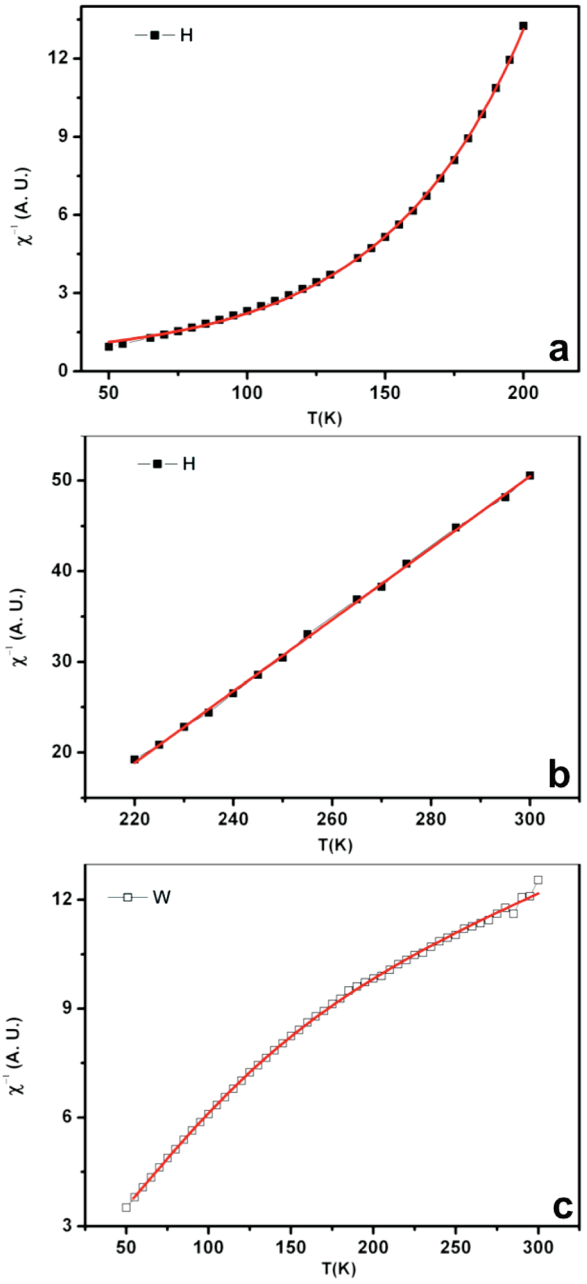

Figure 4. Fits of the inverse susceptibility vs temperature (the PM-temperature range according to eq 4 and the SPM-temperature range by combining eqs 5 and 8) for sample H in the (a) SPM and (b) PM regimes and for (c) sample W.

On the basis of these assumptions, we have carried out fittings of the inverse susceptibility vs temperature for both samples (see for example ref 45 and references therein for a detailed description of using such equations in treating the magnetic properties of a magnetic nanoparticle system). By using eq 4 to fit the PM-temperature range, we have obtained $T_C = 172$ K, and by combining eqs 5 and 8 to fit the SPM-temperature range, we have obtained in this case $T_C = 254$ K and a negligible T_D. Panels a and b Figure 4show the fits for sample H in the SPM and PM regimes, respectively. Although these results are satisfactory and support the proposed SPM-PM transition (the $R^2 = 0.999$ value obtained in both cases corroborates the good agreement between the fits and the experimental data), one has to understand the large difference between the T_C values for the SPM-temperature range ($T_C = 254$ K) and the PM-range ($T_C = 172$ K). We ascribe this difference to the nanoparticles size distribution. For cores and particles in the rough 1−3 nm range, T_C is strongly reduced, and consequently, the different T_C values can be regarded as the lower and upper limits of the T_C distribution.

The $\chi^{-1}(T)$ vs T curve of sample W shows a completely different tendency. To understand such discrepancy we propose two different physical pictures that would explain the decrease of the slope: (a) the overall magnetization of the particle shows a steplike shape, (b) there is an additional magnetic contribution that increases with T. Model a would require the existence of two different magnetic materials at the surface and in the core. Incomplete spin compensations of the AFM state in the oxidized shell would have to be assumed resulting in a very small magnetization and causing an exchange bias. Neither exchange bias nor the existence of two big enough distinct magnetic volumes have been observed in our characterizations. Because model a cannot be experimentally confirmed, we discuss the possible existence of an extra source of susceptibility that gradually increases with T. The origin of this extra contribution can be found in the frustrated spins at the surface of the magnetic particles of sample W. At low temperatures, the contribution of these spins to the particle magnetic moment is negligible, with no appreciable net moment along the field direction. However, with increasing T, these spins will eventually become unpinned and align in the direction of the external field. Although the contribution of these spins should be of the PM type and therefore very small, it can indeed justify the tendency of the magnetization of the ZFC curve that stands for the anomalous behavior of the inverse susceptibility curve, reflected in Figure 3b. Another factor supporting this argument is the temperature-dependence saturation magnetization for sample W at high T, as described below. Although we cannot ascribe this effect to the effective M_S as resulting from two different magnetic phases, we can emphasize the contribution of these "defrozen" surface spins.

On the basis of these results, we have developed a simple model for the depinning probability of one surface spin according to

$$p(T) = f_0 e^{-E_A/k_B T} \tag{9}$$

with k_B the Boltzmann constant, f_0 a normalizing factor, and E_A as the activation energy necessary for the surface spin to become unpinned. We define this dependence in the same way as the probability of one particle to overcome the MAE barrier and switch the magnetization direction. The difference in this case is that (i) it deals with atomic moments instead of particles magnetic moments, and (ii) there is only one energy well of depth E_A. These surface spins behave paramagnetically and their contribution to the total magnetic susceptibility is given by

$$\chi_{PM_{surf}}(T) = \frac{\rho_{AT}(T)\mu_{AT}^2}{3k_B T} \tag{10}$$

where $\rho_{AT}(T)$ is the fraction of surface spins per particle that becomes PM with increasing T. We can assume the fraction of magnetic surface atoms (X_S) of a spherical nanoparticle as a function of the total number of atoms in the particle N_0

$$X_S = \frac{4}{3\sqrt{N_0}} \tag{11}$$

,so that we may approximate the density of spins that can become unfrozen at a given T by

$$\rho_{AT_{surf}}(T) = X_S N \rho_p f_0 e^{-E_A/k_B T} \tag{12}$$

and their contribution to the total susceptibility is given by

$$\chi_{PM_{surf}}(T) = \frac{X_S N \rho_p f_0 e^{-E_A/k_B T} \mu_{AT}^2}{3k_B T} \tag{13}$$

The total susceptibility of the system is computed as the sum of the SPM contribution plus the surface-spins contribution

$$\chi_{total}(T) = \chi_{SPM}(T) + \chi_{PM_{surf}}(T) = \frac{\rho_p \mu_p^2}{3k_B(T+T_D)} + \frac{X_S N \rho_p f_0 e^{-E_A/k_B T} \mu_{AT}^2}{3k_B T} \tag{14}$$

Using $\mu_{AT} = \mu_p/N$ and eq 8, the inverse total susceptibility is given by

$$\chi_{total}^{-1}(T) = \frac{3k_B}{\rho_p \mu_p^2(0)\left[1-\frac{T}{T_C}\right]\left\{\frac{1}{(T+T_D)} + \frac{X_S f_0 e^{-E_A/k_B T}}{NT}\right\}} \tag{15}$$

Considering that the total amount of atoms per particle is $N_0 \approx 2500$, therefore the fraction of magnetic ones (Fe) is 60%, i.e., $N = 1500$, and $X_S \approx 0.034$. Using these values and the above eq 15 we obtain the corrected values $T_D = 32.3$ K, $T_C = 806.0$ K, $E_A/k_B = 616.0$ K and the normalizing factor $f_0 = 6806$ for sample W and a good fit of the experimental data (Figure 4c). $T_D = 32.3$ K indicates a small interaction energy, as evidenced above; the higher $T_C = 806.0$ K is a sign of higher thermal stability, in agreement with the assumption above and $E_A/k_B = 616.0$ K is interpreted as the average temperature for the surface atomic moments to become free and is smaller than T_C, again as expected. This supports our arguments for the existence of frustrated spins at the surface that progressively unpin with increasing temperature and contribute paramagnetically to the total magnetic susceptibility, accounting thereby for the anomalous behavior of sample W.

To further corroborate this discrepancy of the susceptibility behavior to the Curie law, resulting from the dipolar interactions between the nanoparticles in both samples H and W, we have also tested M_S and H_C temperature dependences. In the presence of dipolar interactions,

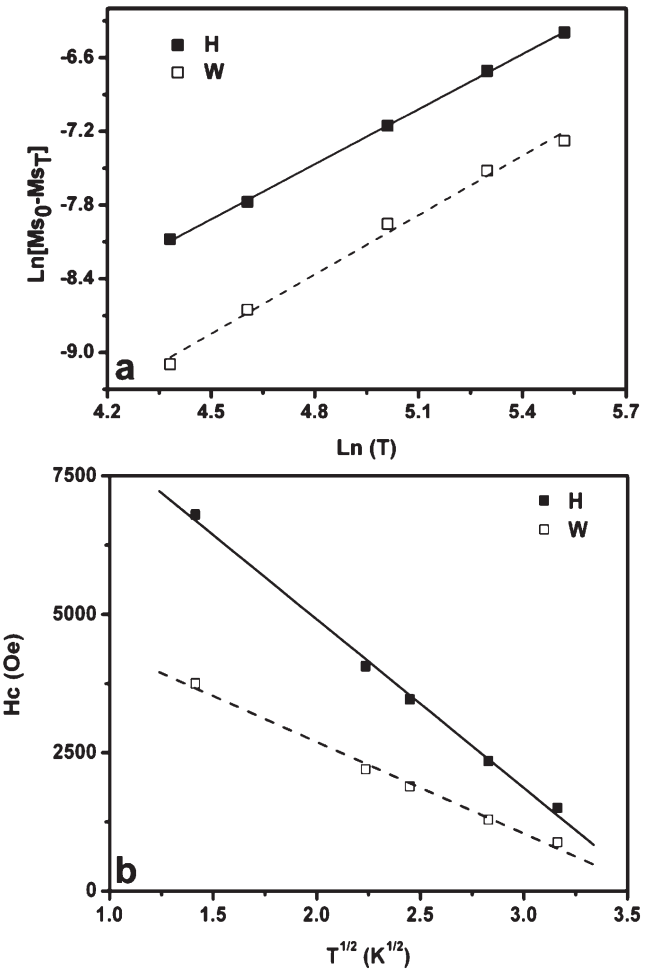

Figure 5. (a) M_S temperature-dependence in the SPM range and (b) H_C temperature-dependence below T_B for samples H and W.

the magnetic susceptibility in the superparamagnetic state, for a system of identical particles of volume V is proportional to

$$M_S^2(T)V/3k_B(T-\theta) \tag{16}$$

where θ is an effective temperature arising from the dipolar interactions.[47] The quantity

$$M_S(T) = \sqrt{\frac{\chi_{SP} 3k_B}{V}(T-\theta)} \tag{17}$$

gives the temperature dependence of M_S, following the conventional law where $M_S(0)$ is the saturation magnetization as T tends to zero and $n = 3/2$

$$M_S(T) = M_S(T=0)[1-\alpha T^n] \tag{18}$$

$M_S(T)$ for both samples H and W were plotted between 80 and 250 K (not shown) assuming a Bloch-law-like temperature dependence (α and $n = 3/2$ are the Bloch constant and Bloch exponent, respectively) to estimate the magnetization $M_S(0)$ of the nanoparticles at $T = 0$ K.

(47) Zitoun, D.; Respaud, M.; Fromen, M.-C.; Casanove, M. J.; Lecante, P.; Amiens, C.; Chaudret, B. *Phys. Rev. Lett.* **2002**, *89*, 037203.

The correctness of assuming Bloch's law[48] is proven by Figure 5a yielding values of $n = 1.494 \pm 0.016$ ($R = 0.9995$) and 1.609 ± 0.078 ($R = 0.9905$) for samples H and W, respectively. The nonlinear behavior of sample W can be understood as a result of the modification of the surface layer. The hydroxide ions attached on the surface of the FePt nanoparticles of sample W induce partial oxidation, causing the demagnetization of the surface spins and consequently the increase in M_S because of this extra source of anisotropy. Therefore, the M_S decrease is smaller that the one predicted by the Bloch law. Although in both samples surface atoms are interacting with the surfactant (oleic acid/oleylamine (H) and TMAOH (W)), the surface layer has apparently become more antiferromagnetically ordered in the second case, promoting frustrated spins in sample W. Thus, the modified temperature dependence of the magnetization for sample W can be attributed to canted surface spins and the reduction rate of the magnetization with increasing temperature is smaller. The fact that the magnetization at the surface is much lower than that of the core at these relatively high temperatures just underlines the presence of disordered surface spins. Additionally, it is important to note that this model works well below the Curie temperature, a condition that is satisfied for sample H and for nanoparticles in a magnetically saturated state.[49,50] Other parameters (θ, n) taking into account stronger dipolar interactions should be considered in the case of sample W.

Below T_B, the FePt nanoparticles exhibit ferromagnetic features including coercivity and remanence. Upon transferring the FePt nanoparticles, the coercivity of the nanoparticles was reduced, consistent with a reduction in the magnetic anisotropy of the nanoparticles. The additional anisotropy in sample W, which increases M_S, contributes only at higher temperatures (for $T > 200$K). At very low temperatures (for $T < 18$ K), the effective magnetic anisotropy for sample W is reduced and can tentatively be attributed to a decrease in the magnetocrystalline anisotropy energy contribution since the FePt core magnetic volume slightly decreases as the oxide is formed. Additionally, at these very low temperatures the extra source of anisotropy with its random axes does not contribute. On the other hand, one may expect an increase in the coercivity taking into account the partial oxidation of FePt nanoparticles. A magnetic exchange coupling induced at the interface between FM and AFM systems could provide an extra source of anisotropy,[51−54] leading to a stable magnetization and larger H_C. Its lack just confirms the incomplete oxidation. Figure 5b shows the temperature dependence of the coercivity. This thermal dependence is expected to follow the equation;

$$H_C(T) = H_C(0)[1 - AT^k] \qquad (19)$$

with $H_C(0)$ the coercive field at $T = 0$ K, and A a parameter which depends on the typical measuring time τ_m and on the effective magnetic anisotropy constant K_{eff}. The exponent k in eq 19 has a value of 0.5 according to the typical Stoner−Wohlfarth model. Figure 5b shows the variation of $H_C(T)$ accordingly, confirming a reasonable fit at low temperatures for both samples.

Conclusion

A complete model for analyzing intrinsic core−shell magnetic properties of nanoparticles is presented. $Fe_{60}Pt_{40}$ nanoparticles stabilized by different ligands (oleic acid/oleylamine or tetramethylammonium hydroxide) and self-assembled in 3D dispersions permit a detailed analysis of the competition of surface, finite-size effects and magnetic interparticle interactions from temperature-dependent magnetometry of the collective magnetic response. Experimental results demonstrate that for FePt nanoparticles with identical size distribution but different surface chemistry, substantial differences of the effective magnetic anisotropy can be determined.

Acknowledgment. D.S. and D.B. thank the Xunta de Galicia Project INCITE 08PXIB236052PR, and the Spanish Ministry of Education and Science project MAT2009-08165. D.S. also acknowledges XdeG for financial support under the *María Barbeito* program and for partially supporting his stay at Universität Duisburg-Essen (PGIDIT-Incite 2009 RHS). D.S. is also indebted to the AGFarle and the Universität Duisburg-Essen. M.S. and M.F. thank the EU-RTN "SyntOrbMag" and "Deutsche Forschungsgemeinschaft, Sfb 445. V.S. acknowledges the financial support of this work under Projects MAT2008-06126 by the Spanish Ministerio de Ciencia e Innovación and INCITE08PXIB209007PR by the regional government (Xunta de Galicia, Spain). V.S. acknowledges the *Ramón y Cajal* Program fellowship (Ministerio de Ciencia e Innovación). The authors also thank the *Centro de Supercomputación de Galicia* computing facilities.

(48) Linderoth, S.; Balcells, L.; Labarta, A.; Tejada, J.; Hendriksen, P. V.; Sethi, S. A. *J. Magn. Magn. Mater.* **1993**, *124*, 269.
(49) Zhang, D.; Klabunde, K. J.; Sorensen, C. M.; Hadjipanayis, G. C. *Phys. Rev. B* **1998**, *58*, 14167.
(50) Aquino, R.; Depeyrot, J.; Sousa, M. H.; Tourinho, F. A.; Dubois, E.; Perzynski, R. *Phys. Rev. B* **2005**, *72*, 184435.
(51) Meiklejohn, W. H.; Bean, C. P *Phys. Rev.* **1956**, *102*, 1413.
(52) Nogués, J.; Schuller, I. K. *J. Magn. Magn. Mater.* **1999**, *192*, 203.
(53) Skumryev, V.; Stoyanov, S.; Zhang, Y.; Hadjipanayis, G.; Givord, D.; Nogués, J. *Nature* **2003**, *423*, 850.
(54) Lund, M. S.; Macedo, W. A. A.; Liu, K.; Nogués, J.; Schuller, I. K.; Leighton, C. *Phys. Rev. B* **2002**, *66*, 054422.